Available online at www.sciencedirect.com
SCIENCE DIRECT
Biochimica et Biophysica Acta 1749 (2005) 173 – 186
BIOCHIMICA ET BIOPHYSICA ACTA
BBA
http://www.elsevier.com/locate/bba

Review

Protein–water displacement distributions

Wolfgang Doster*, Marcus Settles

Technische Universität München, Physik Department E 13 and Institut für Röntgendiagnostik, D-85747 Garching, Germany

Received 3 February 2005; received in revised form 18 March 2005; accepted 18 March 2005
Available online 9 April 2005

Abstract

The statistical properties of fast protein–water motions are analyzed by dynamic neutron scattering experiments. Using isotopic exchange, one probes either protein or water hydrogen displacements. A moment analysis of the scattering function in the time domain yields model-independent information such as time-resolved mean square displacements and the Gauss-deviation. From the moments, one can reconstruct the displacement distribution. Hydration water displays two dynamical components, related to librational motions and anomalous diffusion along the protein surface. Rotational transitions of side chains, in particular of methyl groups, persist in the dehydrated and in the solvent-vitrified protein structure. The interaction with water induces further continuous protein motions on a small scale. Water acts as a plasticizer of displacements, which couple to functional processes such as open-closed transitions and ligand exchange.

Keywords: Protein dynamics; Protein-solvent interactions; Dynamic neutron scattering; Glass transition; Myoglobin

1. Introduction

Understanding protein–water interactions remains one of the major challenges to molecular biophysics. What is the role of the solvent in stabilizing protein structures? Are hydrophilic or hydrophobic forces are dominating [1]? What is the mechanism of dynamic coupling of molecular motions of water and protein structural fluctuations? How does the solvent fit into the picture of the energy landscape of proteins [2,3]?

To answer such questions beyond a pure thermodynamic description requires studying the statistical properties of water and of protein–water interfaces on microscopic scales. In this review, we focus on results obtained mainly with neutron scattering experiments. Dynamic neutron scattering experiments probe the average trajectories of protein and water hydrogen atoms in space and time. The wavelength of thermal neutrons, typically 5 Å corresponds to intermolecular distances and the experimentally recordable velocity changes of the scattered neutrons cover a time window ranging from femtoseconds to nanoseconds. Thus, low frequency vibrations, molecular displacements on the scale of protein–water hydrogen bond fluctuations up to collective diffusion can be studied. Since the scattering cross-section of the hydrogen nucleus is about ten times larger than those of other nuclei in proteins, including deuterium, one can focus either on protein-internal motions or hydration water depending on whether one chooses D_2O or H_2O as solvent. In the former case, one probes the average displacement of all non-exchangeable hydrogens of protein side chains. Neutron scattering is thus a suitable method to record collective motions. To be more selective, one can deuterate particular domains or sidechains [4]. To reduce the scattering from the bulk solvent phase, one often works with very concentrated solutions or hydrated systems. Since we are interested in the role of water, mostly hydrated proteins will be discussed. In solution, translational and rotational motion of the entire protein molecule complicate the spectrum.

We are thus concerned with environments resembling those of protein crystals. In fact protein crystals are very suitable samples for neutron scattering experiments, complementing static X-ray crystallography. With neutrons, one measures thermal diffuse (incoherent) scattering which is orders in magnitude less intense than Bragg reflections. Thus, relatively large samples, typically 50 to 100 mg of

* Corresponding author.
E-mail address: wdoster@ph.tum.de (W. Doster).

1570-9639/$ - see front matter © 2005 Elsevier B.V. All rights reserved.
doi:10.1016/j.bbapap.2005.03.010

(non-crystalline) material is required. Using the method of 'elastic resolution spectroscopy' much smaller samples become feasible [5,6]. For each atom i, one can determine a displacement distribution function $G_i(\vec{r},t)$. It denotes the probability distribution that a particular atom performs a displacement '$\vec{r}_i$' in time 't'. Experimentally one measures the scattering function versus momentum and energy exchange, $S(\vec{q},\hbar\omega)$ averaged over all atoms. The protein–water displacement distribution function can be reconstructed from its moments using neutron scattering data. The interpretation of such data is facilitated by molecular dynamics simulations. For instance, the second moment, the mean square displacement is a basic result of MD simulations [7,9–12]. Equilibrium displacement distributions of proteins have been derived from temperature factors of the Bragg reflections using x-ray crystallography [13,14,18]. This provides spatially-resolved mean-square displacements of each residue. With incoherent neutron-scattering one probes a time-resolved, spatially-averaged displacement distribution. Protein–water dynamics studied by neutron scattering has been reviewed in ref. [7,17,19].

2. Water-plasticized protein structural motions

From a dynamical point of view, liquids and proteins are radically different: Liquids exhibit short-range order and long range translational diffusion. Molecular displacements in liquids are continuous and isotropic. Proteins in contrast are long-range ordered, but molecular diffusion is of short range. Internal displacements are discontinuous, rotational and anisotropic. Generally, motion in dense systems is controlled by short-range repulsive interactions. A molecule can only move if the nearest neighbors also move. This is a collective phenomenon resembling a continuous search for escape out of a cage rather than a discontinuous jump across an energetic barrier. Bypassing the barrier by collecting sufficient free volume rather than barrier crossing appears to be the dominant diffusion mechanism in the liquid state [20,21]. The cage becomes a trap when the density reaches a critical value. Then, the liquid is arrested on a macroscopic scale. Rotational motions involve smaller volume changes than translation. Thus, torsional transitions occur even in dense systems such as proteins. Moreover, the protein–water interaction causes the torsional barriers to fluctuate. The protein–water coupling thus introduces liquid aspects to otherwise solid-like molecules. From a polymer physics point of view, water acts as a plasticizer to protein motions [23–25], expanding the accessible protein conformational space by decreasing friction and effective barrier heights. Dehydration thus leads to an 'infinite viscosity' or glassy state [24,26]. 'Glassy' implies the absence of long and intermediate range diffusion. Thus, diffusion of small molecules across the protein surface is suppressed, while intra-molecular displacements are not hindered: kinetic studies of ligand binding to myoglobin in viscous liquids show that the ligand transfer rates across the protein–solvent interface decrease with increasing solvent viscosity. But intra-molecular ligand binding remains unaffected by increasing solvent friction [16].

The loss of surface plasticity derives from an indefinite increase in the solvent relaxation time τ_η. The Maxwell relation links the structural relaxation time τ_η and the shear viscosity of a liquid η by [28]:

$$\eta = G_\infty \cdot \tau_\eta \tag{1}$$

τ_η is the relaxation time of a visco-elastic oscillator and $G_\infty \propto \omega_0^2$ denotes the high-frequency elastic modulus of the liquid. The glass transition is defined by the temperature T_G, where τ_η has reached a time scale of 100 s or $\eta = 10^{13}$ Poise. Solvent relaxation times and the effect of viscous protein–solvent coupling to ligand binding have been discussed in [16]. Fig. 1 shows that the glass temperature of the collagen–water system decreases with increasing water content [27]. Below T_G proteins are solid-like, rigid molecules. Only rotational transitions of side-chains, resembling those in molecular glasses, occur. Above T_G, proteins exhibit rubber-like plasticity: Structural fluctuations can be of medium range, but the equilibrium native structure is restored by entropic elasticity. Protein structures are composed of ordered regions, α-helices and β-sheets, which are connected by disordered turns. From this point of view, protein molecules, like partially crystalline polymers, could be pictured as 'fringed micelles' [23]. Water will preferentially penetrate the disordered fringes, inducing swelling and plasticization. The resulting decrease in protein density activates liquid-like translational displacements of side-chains in excess to rotational transitions. The extra translational mobility allows the side-chains to move out of the way, enabling the diffusion of small ligand molecules across an otherwise close-packed structure. Fig. 2 illustrates how in the dry system, hydrogen bonds have to be saturated internally, while water molecules offer alternative binding sites which opens the structure. Water thus introduces fluctuations, reducing the entropy and destabilizing the native state. This

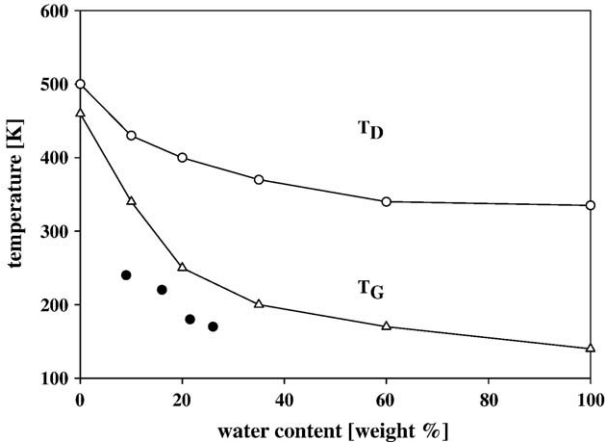

Fig. 1. Glass temperature (T_G) and denaturation temperature (T_D) of hydrated collagen versus water content [27] and onset-temperature of diffusive motion in lysozyme on a 50-ps time scale, full circles [29].

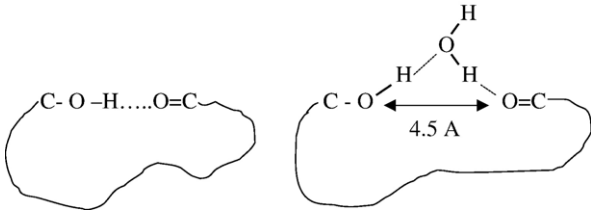

Fig. 2. Protein–water interaction: without water (left) hydrophilic interactions have to be saturated internally, right: water allows the structure to expand, the optimal hydrogen bond configuration for the coupling of two functional sites is shown [22].

is why the denaturation temperature T_D in Fig. 1 decreases with increasing water content. Thus, 'lubricating' protein motions appears to be the main role of water. The figure also shows the onset temperature of anharmonic motions in lysozyme versus degree of hydration measured with neutron scattering on a 50-ps time scale [29]. The trend is the same, but the data suggest that the onset of fast motions occurs at lower temperatures than the global relaxation process.

Fig. 3 shows the neutron scattering function $S(q, \Delta E = \hbar\omega)$ of myoglobin exposed to three types of environment: vacuum (dehydrated), fully hydrated with D_2O (0.35 g/g) and vitrified in a perdeuterated glucose glass [30].

The wings of the protein spectra appear to be broadened with respect to the resolution function, which is the signature of structural fluctuations on a picosecond time scale. The dehydrated and the glucose-vitrified protein exhibit almost identical spectral broadenings, suggesting the existence of internal motions, which occur irrespective of the nature of the solvent. The excess broadening of the hydrated protein is the result of water-plasticized translational motions of side chains. Not only the spectral properties, but also the spatial features of theses two types of displacements differ. The spatial information derives from the angular dependence of the neutron scattering spectrum as will be discussed below [37].

Protein dynamics observed by dynamic neutron scattering is a classical topic, which has been discussed by several authors, just to give a small collection [29,31–36]. The relation between liquids and proteins was discussed in [12,15,17,63]. The glass transition of hydration water is known to trigger the onset of anharmonic protein motions, observed with Mössbauer and neutron spectroscopy since 1986 [37–39].

3. Properties of the dynamical structure factor

Neutrons are scattered by the nuclei, which are point-like entities. The respective scattering amplitudes depend on the individual nuclear cross-sections [40,41]. For the present purpose we focus on the protein hydrogens, since they comprise roughly 90% of the total cross-section. Replacing ^1H by ^2H allows reducing the cross-section of the exchangeable hydrogens by a factor of ten. Myoglobin includes ca. 1000 carbon-bound (non-exchangeable) hydrogens, 130 hydrogens are surface-bound exchangeable, and ca 150 are amide protons. Some of those (75) are buried and slowly exchanging. The fully hydrated protein (0.35–0.4 g/g) also includes 700–800 water protons. Since the cross-section depends on the relative neutron–proton spin orientation, which is random, waves originating from different atoms do not interfere. The scattering signal is thus incoherent, implying a superposition of intensities and not of amplitudes. Translational motion of the scattering center modulates the phase of the wave train. The phase correlations in time thus reflect the average trajectory of individual particles, sometimes called 'self-interference'. As the central experimental quantity we introduce the self-intermediate scattering function, $I_{s,j}(\vec{q}, t)$, which can be defined for each atom j separately:

$$I_{s,j}(\vec{q}, t) = \langle \exp\left(i\vec{q} \cdot \vec{r}_j(0)\right) \cdot \exp\left(-i\vec{q} \cdot \vec{r}_j(t)\right)\rangle, \qquad (2)$$

$q = 4\pi\sin(\theta/2)/\lambda$ denotes the modulus of the scattering vector. λ is wavelength of the incident neutrons and θ is scattering angle. The brackets denote an average covering the initial times. The scattering experiment is sensitive to correlated phase fluctuations. One thus observes displacements projected onto the wavevector $\vec{q}$, which is an experimental parameter. By varying λ and θ, one varies the spatial (and temporal) resolution of the instrument. Note the absence of phase correlations between different atoms (i, j) as a consequence of the random phase approximation. With D_2O-hydrated protein samples, we ignore about 5–10% coherent scattering. In solution however, coherent scattering by D_2O dominates. The displacement distribution function is then derived from the intermediate scattering function by a Fourier transform:

$$G_{s,j}(\vec{r}, t) = \int \frac{d^3q}{(2\pi)^3} \exp(-i \cdot \vec{q}\,\vec{r}) \cdot I_{s,j}(\vec{q}, t). \qquad (3)$$

This even function in space (and time) [40] describes the single particle dynamics of a system averaged over the possible starting points in space. It denotes the probability density, that atom (j) which is initially at $\vec{r}_0$ moves to a

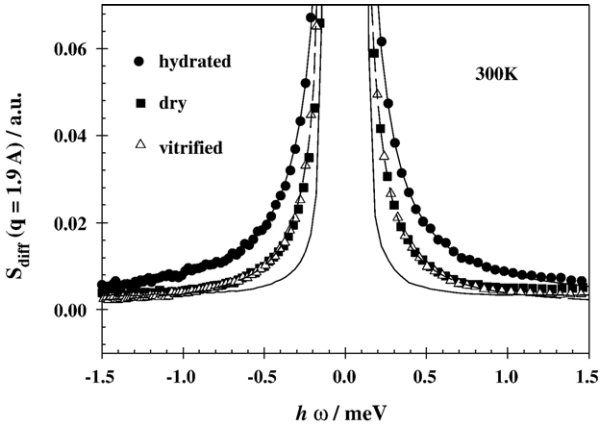

Fig. 3. Neutron scattering spectra of myoglobin embedded in three environments: 0.35 g D_2O/g, 0.05 g/g and 1 g/g in perdeuterated glucose (dehydrated), (q = 1.9 Å^{-1}, 1 meV = 8 cm^{-1}). Full line: instrumental resolution function (IN6, ILL). A vibrational background was subtracted [30].

position $\vec{r}$ within a time interval t: For a classical system it can be written as:

$$G_{s,j}(\vec{r},t) = \int d^3r_0 p(\vec{r}_0+\vec{r},\vec{r}_0,t)\cdot p_0(\vec{r}_0), \tag{4}$$

with the equilibrium distribution

$$p_0(\vec{r}) = p(\vec{r},\vec{r}_0,t=\infty). \tag{5}$$

Thus, the q-dependence of $I_{s,j}(\vec{q},t_{res})$ contains the complete information about the single particle dynamics at any fixed instant of time $t = t_{res}$ (often defined by the energy resolution of the instrument). This argument is stressed, because the intermediate scattering function is usually introduced as a correlation function versus time or spectrum versus frequency for fixed values of q, which leads to the well-known effects of q-dependent lineshapes and linewidths. In the following, we omit the subscript 's' and average over all hydogens j. The interpretation of experimental data becomes most transparent in the case of small q and/or short times, as can be seen from the expansion of$I\ (\vec{q},t)$ in powers of q^2:

$$I(\vec{q},t) = \int d^3r \exp(-i\vec{q}\,\vec{r})\cdot G_s(\vec{r},t) \tag{6}$$

$$= 1-\frac{1}{2}\cdot q^2\cdot\langle(\hat{q}\,\vec{r})^2\rangle(t) + \frac{1}{24}\cdot q^4\cdot\langle(\hat{q}\,\vec{r})^4\rangle(t) - O(q^6), \tag{7}$$

with $\vec{q} = q\cdot\hat{q}$. This is the moment (Plazcek) expansion of the displacement distribution $G(r, t)$. In the limit:

$$q^2\langle(\hat{q}\,\vec{r})^2\rangle(t) \ll 1 \tag{8}$$

only the first term of the expansion contributes and two essential consequences arise:

1. the correlation function and spectrum are completely determined by the mean squared displacement and
2. the intermediate scattering function and dynamic structure factor factorize into a term $\propto q^2$ and a purely time or frequency dependent function, respectively: [1]

$$I(\vec{q},t) = 1-\frac{1}{6}\cdot q^2\cdot\langle r^2(t)\rangle \tag{10}$$

$$S(\vec{q},\omega) = \delta(\omega)+\frac{1}{6}q^2\cdot \mathrm{FT}\{-\langle r^2(t)\rangle\}(\omega) \tag{11}$$

The delta function is included for mathematical consistency only. Displacements in simple cases, the harmonic oscillator, ideal gases and regular diffusion, are Gaussian distributed. But density fluctuations in complex systems such as liquids and proteins are rarely Gaussian. In this context, we introduce various non-Gaussian models.

[1] Let us – for notational simplicity – assume the usual case of an isotropic sample (not necessarily isotropic dynamics!, see below) which leads to the orientational average of the scalar products in the displacement moments:

$$\frac{1}{4\pi}\int d\Omega\langle(\hat{q}\,\vec{r})^{2n}\rangle(t) = \frac{1}{2n+1}\langle r^{2n}(t)\rangle \tag{9}$$

4. Non-Gaussian displacement distributions

A Gaussian distribution in space, $G(\vec{r},t)$ implies a Gaussian $I(\vec{q},t)$, averaged over all atoms (j) at any instant of time [42]:

$$I(\vec{q},t) = \exp\left(-\frac{q^2}{2}\cdot w(t)\right) \leftrightarrow G(\vec{r},t) = (2\pi w(t))^{-3/2}\cdot\exp\left(-\frac{r^2}{2w(t)}\right) \tag{12}$$

where the width function is defined by:

$$w(t) = \frac{1}{3}\cdot\langle r^2(t)\rangle \tag{13}$$

The physical origin causing a deviation from Gaussian behavior can be either extrinsic or intrinsic. To quantify the deviation, we expand the intermediate scattering function, Eq. (7), up to q^4, assuming the sample to be isotropic:

$$I(q,t) = 1 - B(t)\cdot q^2 + C(t)\cdot q^4 \tag{14}$$

with $B(t) = 1/6\ \langle r^2\rangle$ and the curvature is characterized by the Gauss deviation $g(t)$:

$$g(t) := \frac{C(t)}{B^2(t)} \tag{15}$$

which equals 1/2 in the case of a Gaussian distribution.

4.1. Intrinsic deviation

(1) The geometrical constraints imposed by the covalent structure of a polypeptide chain restricts the number of allowed conformations. For instance, the three positions of a methyl group or alternate values of the main and side-chain dihedral angles lead to discrete distributions. The respective intermediate scattering function decays to a finite plateau at long times, which depends on q. The structure factor for a three-fold rotation is given by [40]:

$$S_3(q) = I(q,t\to\infty) = \frac{1}{3}\left(1+2\cdot\frac{\sin(q\sqrt{3}r)}{q\sqrt{3}r}\right) \tag{16}$$

where r denotes the length of the $C–H$ vector in the case of a methyl group.

(2) The granular nature of matter and close-packing lead to deviations from Gaussian behavior even in simple isotropic liquids on a microscopic scale: Each particle is surrounded by a cage formed by its nearest neighbors. At low densities, the smooth diffusional dynamics lead to a Gaussian displacement distribution at all times. However, on approaching the viscous liquid regime, the motional constraints due to the cage effect together with the retarded

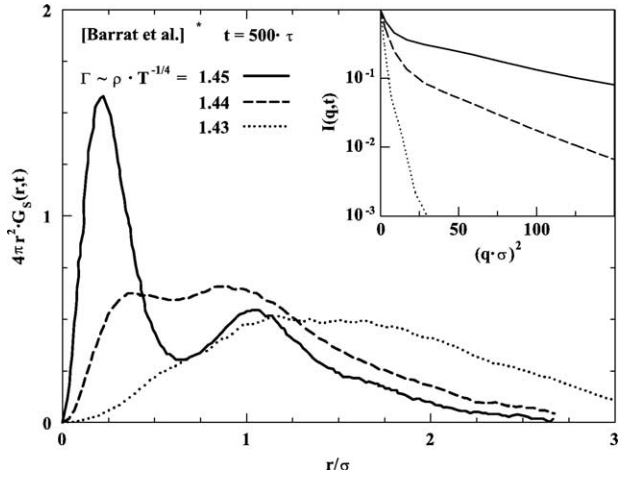

Fig. 4. Displacement distribution function of a Van der Waals liquid (radius σ) at fixed time and variable density. Insert: corresponding intermediate scattering functions versus q [43].

escape from the latter lead to an essentially bimodal distribution of displacements on the escape time scale. An example is given by a molecular dynamics simulation by Barrat et al. [43] of a Van der Waals liquid shown in Fig. 4: The splitting into a fraction of particles having left their cage and the rest, which still resides inside, in a sense represents a special case of a bimodal distribution of motional amplitudes. The same effect is seen in a simulation of water by Sciortino et al. [44].

4.2. Extrinsic deviation [42]

These are defined by distinct q-profiles from different atoms of an ensemble due to a distribution of motional amplitudes (inhomogeneity) or due to anisotropic motion:

• *Inhomogeneity*. If an ensemble is, at a certain time t_{res}, characterized by a normalized distribution of width functions $f(w, t_{res})$ of otherwise isotropic Gaussian dynamics, then the expansion reads:

$$I(q,t_{res}) = \int dw f(w,t_{res}) \cdot \exp\left(-\frac{1}{2}q^2 w\right) = 1 - \frac{1}{2}q^2\langle w\rangle(t_{res}) + \frac{1}{8}q^4\langle w^2\rangle(t_{res}) + O(q^6)$$

thus,

$$g(t_{res}) = \frac{1}{2}\cdot\frac{\langle w^2\rangle(t_{res})}{\langle w\rangle^2(t_{res})} \tag{17}$$

i.e., the Gauss deviation is determined by the relative squared width of the distribution.

• *Anisotropy*. If one assumes, just to illustrate the essential effects, a rotational ellipsoid of mobility, one obtains:

$$G(\vec{r},t) \sim \exp\left(-\frac{x^2+y^2}{2w_{xy}(t)}\right)\cdot\exp\left(-\frac{z^2}{2w_z(t)}\right), \tag{18}$$

the Fourier transform of this equation is given by:

$$I(\vec{q},t) = \exp\left(-\frac{1}{2}q^2 w_{xy}(t)\right) \cdot \exp\left(-\frac{1}{2}q^2\left(w_z - w_{xy}(t)\right)\cdot\cos^2\theta\right), \tag{19}$$

where θ denotes the angle between $\vec{q}$ and the z-direction. Performing the orientational average for a powder sample yields:

$$I(q,t) = \exp\left(-\frac{1}{2}q^2 w_{xy}(t)\right)\cdot\frac{\sqrt{\pi}}{2}\cdot\frac{\operatorname{erf}\left(\frac{q}{\sqrt{2}}\sqrt{w_z(t)-w_{xy}(t)}\right)}{\frac{q}{\sqrt{2}}\sqrt{w_z(t)-w_{xy}(t)}}, \tag{20}$$

with a correspondingly complex argument of the error function in the case of an oblate mobility ellipsoid ($w_{xy}(t) > w_z(t)$). erf(x) denotes the error function. For small q, Eq. (20) starts off as a Gaussian:

$$I(q,t) = 1 - \frac{1}{6}q^2\left(2w_{xy}(t) + w_z(t)\right), \tag{21}$$

but decays only algebraically for large arguments in the case of purely one- or two- dimensional dynamics:

$$I(q,t) \overset{\text{arg}\gg 1}{\sim} \begin{cases} q^{-2}\cdot w_{xy}^{-1}(t) & \text{for } w_z(t) = 0 \\ q^{-1}\cdot w_z^{-1/2}(t) & \text{for } w_{xy}(t) = 0. \end{cases} \tag{22}$$

Expanding Eq. (20) further leads to the Gauss deviation:

$$g(t) = \frac{1}{2}\cdot\frac{1 + \frac{2}{3}\left(\frac{w_z(t)}{w_{xy}(t)} - 1\right) + \frac{1}{5}\left(\frac{w_z(t)}{w_{xy}(t)} - 1\right)^2}{1 + \frac{2}{3}\left(\frac{w_z(t)}{w_{xy}(t)} - 1\right) + \frac{1}{9}\left(\frac{w_z(t)}{w_{xy}(t)} - 1\right)^2}, \tag{23}$$

shown in Fig. 5 as a function of the axial ratio, w_z/w_{xy}, of the displacement ellipsoid.

Isotropic motion is characterized by a Gauss-deviation of 0.5, values near 0.6 indicate two-dimensional displace-

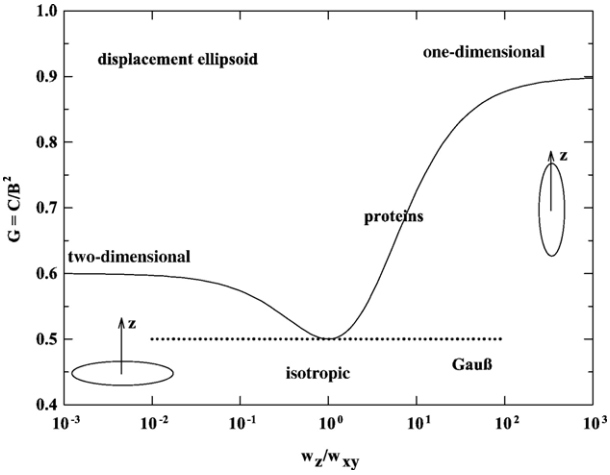

Fig. 5. Gauss-deviation, g, due to anisotropy: ellipsoid of displacements versus axial ratio, experimental values with proteins range near 0.6–0.7.

ments, while 1-dimensional motion leads to $g(t) = 1$. For proteins, we observe typically $g = 0.6–0.7$ indicating slightly skewed two-dimensional motion. All these effects may contribute to the observed non-Gaussian displacement distribution in proteins.

5. Distribution of protein structural fluctuations

Which of the above models now applies to protein motions? As shown above, the relevant spatial information is contained in the q-dependence of the intermediate scattering function $I(q, t)$. We first consider data at fixed time versus the temperature. In the next section, we explicitly include the time evolution. Fig. 6 shows $I(q, t)$, at $t_{res} = 50$ ps for myoglobin in three environments: dehydrated, vitrified and fully hydrated.

Linear plots of log $I(q, t)$ versus q^2 indicate Gaussian displacements as for vibrational motions at low temperatures. Above about 200 K non-Gaussian deviations become significant [37]. The structure factors of the dry and vitrified sample differ little, suggesting similar types of intra-molecular motions, consistent with the energy resolved experiment in Fig. 3. The hydrated protein shows an additional decrease in the structure factor at fixed time, indicating further reorientation and loss in spatial correlations due to water-assisted motions. The minimal model of protein displacements thus involves two Gaussian components 1 and 2 [17,42,46]:

$$I(q,T,t_{res}) = A_1 \cdot \exp\left(-q^2\langle\Delta x_1^2\rangle/2\right) + A_2 \cdot \exp\left(-q^2\langle\Delta x_2^2\rangle/2\right) \quad (24)$$

Note that $\langle r^2\rangle = 3\langle\Delta x^2\rangle$. Fig. 7 shows the second moments of the two Gaussian components determined on absolute scale [17,37].

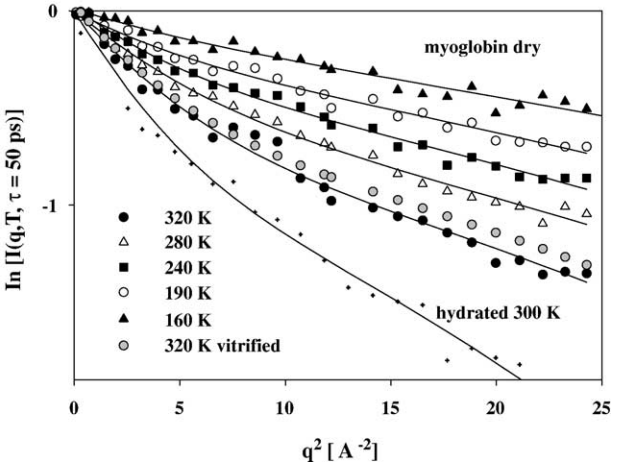

Fig. 6. Intermediate scattering function at fixed time, $I(q, t_{res} = 50$ ps), versus q and temperature for dry myoglobin. Selected data of glucose-vitrified and D_2O-hydrated myoglobin (0.35 g/g) are also shown, lines: fit using Eq. (16), instrument: IN13, ILL, [37,45].

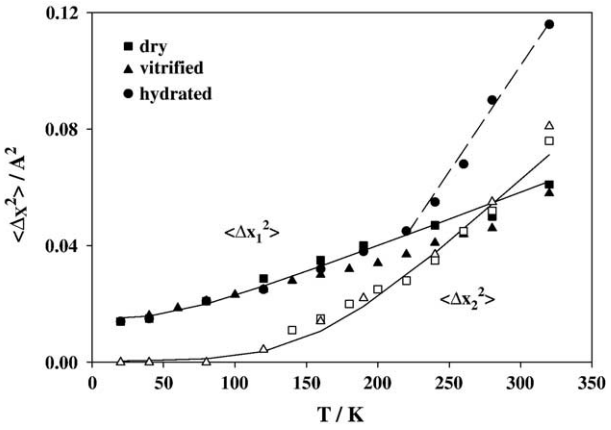

Fig. 7. Second moment of the displacement distribution including the zero-point vibration (myoglobin, dry, D-glucose-vitrified and hydrated (0.35 g/g) at a fixed time of 50 ps, derived from data in Fig. 6. Closed symbols: component 1(vibration + water-induced), open symbols: component 2 (torsion), lines: from fits in Fig. 6, dashed: dynamical transition. Instrument: IN13, ILL.

The first component (1) exhibits a low temperature plateau below 20 K, which carries the zero point vibrations of myoglobin. The displacements at higher temperatures are compatible with harmonic behavior up to 320 K in the case of dehydrated and the vitrified myoglobin. However, in the hydrated system, a strong increase occurs above 240 K suggesting water-assisted motions. The second component (2) emerges at 150 K, implying a nonlinear enhancement in the total displacements independent of the protein environment. By contrast in experiments with trehalose-coated myoglobin, harmonic behavior was reported [47]. With D-exchanged glucose (instead of perdeuterated), we get a similar result because of a large contribution from the glassy matrix.

Fig. 8 shows our central result: a reconstructed displacement distribution, $4\pi r^2 G(r,t)$, of hydrated myoglobin versus temperature. Its bimodal shape is reminiscent of a liquid (Fig. 4). Component (1) broadens with increasing temperature due to vibrational motions. But above 240 K, the maximum is

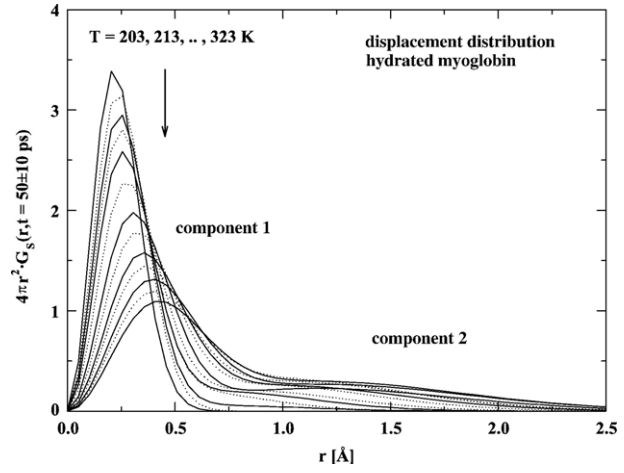

Fig. 8. Displacement distribution (myoglobin, D_2O-hydrated (0.35 g/g)) at a fixed time (50 ps) versus temperature derived from data in Fig. 6, instrument: IN13, ILL.

shifting and the width increases. This effect is seen only with hydrated samples and indicates enhanced motional amplitudes on a small scale. In contrast, component (2) is observed in all samples independent of the protein environment. It corresponds to larger scale excursions suggesting rotational jumps of side chains.

What is the molecular nature of the two types of motions? Several authors have emphasized the relevance of dynamical heterogeneity in the context of neutron scattering experiments [7,46]. We have attributed the non-Gaussian scattering function to torsional jumps, which was supported by an early simulation of hydrated myoglobin by Loncharich and Brooks [37,62].

Rotational jumps of methyl groups and of heavy atom dihedral transitions are the most natural modes of motion of a polypeptide chain. Moreover the partial cross-section due to methyl groups is typically 25%, which is the largest individual contribution of a molecular group. If the partial cross-section, the structure factor, the barrier to rotation from energy-resolved experiments (Fig. 3) and the instrumental resolution function are known, one can calculate the intermediate scattering function at t_{res} without adjustable parameters:

$$I(q,t_{res}) = \exp(-2W)\cdot[S_3(q) + (1 - S_3(q))\cdot R(t_{res})] \quad (25)$$

W denotes the Debye–Waller factor (Gaussian) and $S_3(q)$ is orientationally averaged incoherent structure factor of a three-fold torsional jump (Eq. (16)). Assuming a Gaussian resolution function of energy width σ convoluted with a Lorentzian spectrum (correlation time τ), yields following $R(t_{res} \approx \hbar/\sigma)$ [5,6]:

$$R(\sigma,\tau) = erfc\left(\frac{\hbar}{\sqrt{2}\sigma\tau}\right)\cdot \exp\frac{\hbar^2}{2\sigma^2\tau^2} \quad (26)$$

The R-function is unity for $\sigma\cdot\tau/\hbar \gg 1$ and vanishes in the opposite limit, when the process is fully resolved by the instrument.

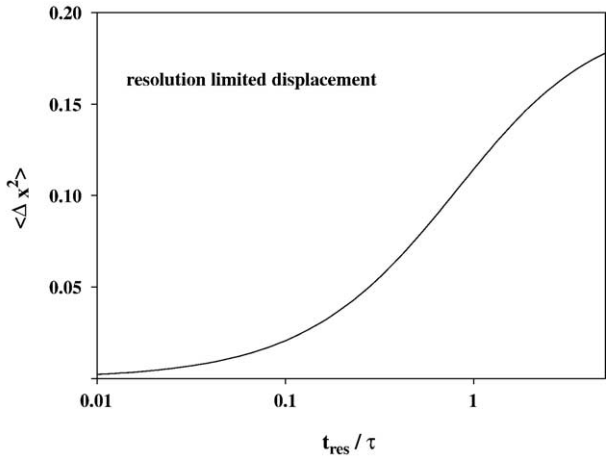

Fig. 9. Mean square displacement versus correlation time $\tau[T,\eta)$ at fixed resolution, t_{res}, according to Eq. (27) for $\langle\Delta x^2_{conf}\rangle = 0.2$ Å^2.

The effective displacements depend through σ and $\tau(T)$ on the instrumental properties and the relaxation time of the molecular process:

$$\langle\Delta x^2_{eff}\rangle = \langle\Delta x^2_{vib}\rangle + \langle\Delta x^2_{conf}\rangle\cdot(1 - R(\sigma\cdot\tau)) \quad (27)$$

An example is shown in Fig. 9, where the displacement increases because of a diminishing relaxation time $\tau(T)$. The nonlinear onset thus occurs in the range of $t_{res}/\tau = 0.2$. Here, we discriminate two types of temperature dependent processes: Barrier-controlled transitions, which exhibit an Arrhenius temperature dependence in $\tau(T)$ and solvent-controlled processes, which exhibit a super-Arrhenius behavior, $\tau(\eta)$. Only the latter contribute to the dynamical transition. In this case, the effective displacements vanish with the diverging viscosity of the solvent. The average rotational barrier of methyl groups in myoglobin is in the range of 10 kJ/mol [6,17,48]. The solid lines in Figs. 6 and 7 represent fits assuming tortional transitions of methyl groups to be the dominant molecular process. The reasonable agreement with experimental data produced by the model suggests that rotational transitions, essentially of methyl groups, are likely to be the origin of the non-Gaussian displacement distribution. Dynamical heterogeneity seems to be of minor importance. Torsional transitions occur in the hydrated, the dry as well as in the vitrified state. The rates may differ however. The increase in rotational speed of methyl groups with rise in temperature follows an Arrhenius law. This should not be confused with a dynamical transition, where the rate of a dynamic variable, water reorientation at the protein surface, varies in a super-Arrhenius manner. The apparent displacements of component 2, $\langle\Delta x^2_2\rangle$, in Fig. 7, should be interpreted as arising from an increasing rotational rate $1/\tau$ at fixed instrumental resolution σ (Fig. 9). This result is closely related to the general increase in the displacements of methyl groups with temperature observed with NMR for lysozyme [49]. The slight discrepancy between the data and the theoretical curve at low temperatures may reflect a distribution of rates.

Water induces additional small-scale protein displacements, which appear as anharmonic enhancements of the vibrational component 1 (Fig. 7). Thus, in contrast to a liquid displacement distribution, large-scale excursions reflect the solid aspect of protein motions, while the liquid aspect resides in small-scale continuous displacements. The moment analysis suggested a quasi two-dimensional average displacement. A possible interpretation based on the methyl side-chain as reporter group could be, that apart from a rotation about the C–C axis, a librational motion occurs about an axis perpendicular to rotation. The latter is water-induced and contributes to the observed Gauss-deviation as indicated in Fig. 5.

The basic two-state model may be replaced by an effective three-state model. Originally, amplitude fluctuations of fast hydrogen bond motions in asymmetric wells

were assumed to create the anharmonic increase in the displacements [37]. While this still holds on a picosecond time scale (IN6) [17], back-scattering spectrometers (IN13) can resolve slower rotational motions, which contribute further to the effective displacements. Such low-flux, high-resolution spectrometers are not sensitive enough to detect fast H-bond switching, the basic mechanism of the dynamical transition.

As an alternative approach to analyze the second moments a so-called force-constant model was proposed by Zaccai and Bicout [4,50]: inspired by vibrational motions, the apparent slope of the temperature dependence of anharmonic displacements is interpreted in terms of an effective force constant D_{eff} defined by: $\langle \Delta x^2_{\mathrm{conf}} \rangle = k_B T / D_{\mathrm{eff}}$, which is still correct for an overdamped Brownian oscillator. The most severe limitation of this model is to ignore the effect of a finite observation time t_{res} (Fig. 9). The force constant model applies therefore only to motions, which are much faster than t_{res}. Daniel et al. [8,52] claim to observe enzymic activity on a time scale of seconds and temperatures well below the dynamical transition, which is studied a picosecond time scale. That structural fluctuations become invisible on a picosecond time scale has in general little impact on processes which are ten orders in magnitude slower. Such statements have thus little physical meaning except in the vicinity of a glass transition: within 10 or 20° near the glass temperature a structural relaxation time can diverge from microscopic values to hundreds of seconds.

6. Time-resolved displacements of protein hydration water

In the following, we discuss neutron scattering spectra derived from H_2O-hydrated and -solvated myoglobin, where the water of hydration yields the dominant

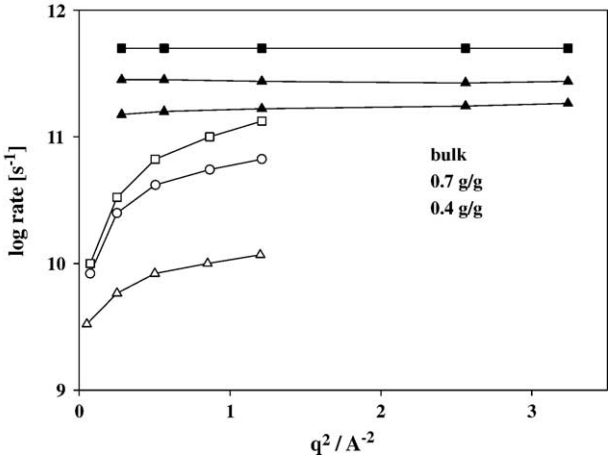

Fig. 10. Lorentzian rates derived from a two-component analysis of neutron scattering spectra of bulk and protein hydration water (H_2O-hydrated myoglobin at 293 K, instruments: IN6 and IN15 ILL, Grenoble) [53,54,45].

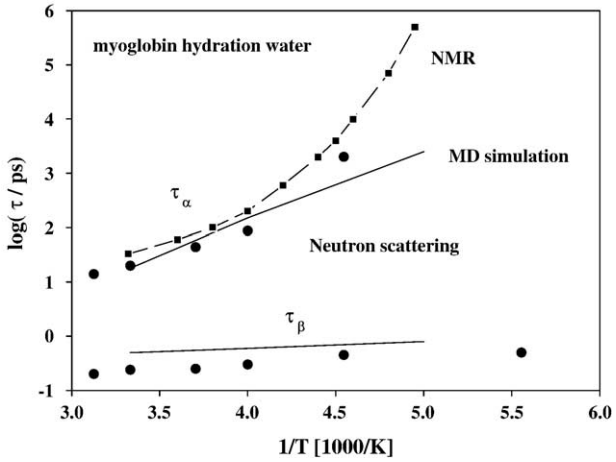

Fig. 11. Protein–water relaxation times versus temperature, D_2O-hydrated myoglobin 0.35 g/g, comparing ^{2}H-NMR, neutron scattering data and MD simulations [9,10,54,55].

contribution. In a conventional data analysis one fits the scattering function $S(q, \omega)$ as a sum of Lorentzian spectra, which are convoluted with the resolution function of the instrument. For H_2O-hydrated myoglobin as well as for bulk water a minimum of two spectral components (possibly rotation and translation) are required to fit the data [53].

Fig. 10 shows the resulting rates versus q, comparing bulk water and hydration water at 0.4 g/g (hydrated) and 0.8 g/g (solvated) [54]. The water mobility increases continuously with distance from the protein surface.The rate of the fast component (2–6 ps) is independent of q and thus independent of the probing spatial scale. This is a characteristic feature of local motions. The rate enhancement with distance from the protein surface may be pictured as a smooth transition from flip–flop motions between bound water states, to hindered and free rotational diffusion. The rate of the slow component increases with q^2 but approaches a plateau at high q. The plateau denotes the rate of discrete steps, while at low q many translational steps occur, leading to diffusion. Again, the rate at fixed q increases continuously with distance from the protein surface approaching the bulk value within three to four water layers. Due to the presence of a 'wall', the relaxation rate of hydration water is reduced at room temperature by a factor of 10 relative to bulk water. The respective viscosity is then according to Eq. (1) enhanced by the same factor.

Fig. 11 compares the relaxation times of hydration water using derived from ^{2}H-NMR, neutron scattering and simulation versus reciprocal temperature. Neutron scattering data and simulation reveal a fast β-process, whose correlation time is nearly temperature independent. The structural relaxation time related to translation of hydration water varies however in a super-Arrhenius manner with temperature as the neutron scattering and the deuteron relaxation data demonstrate. These results provide evi-

dence that hydration water turns into a glassy state near 200 K. Approximating $\tau_w(T)$ by a Vogel–Fulcher law:

$$\tau_w = \tau_0 \cdot \exp\left(\frac{A}{T - T_0}\right) \tag{28}$$

yields the following parameters: τ_0 = 1.0 ps, A = 3.3 kJ/mol and T_0 = 170 K, suggesting a critical temperature near 180 K. The onset temperature of water-induced protein displacements in Fig. 7 is 240 K. The respective water correlation time amounts to τ_w = 300 ps. From Fig. 9, we take the onset condition, t_{res}/τ_p = 0.2. For t_{res} = 50 ps, this yields an estimate for τ_p = 250 ps ≈ τ_w at the onset temperature. The super-Arrhenius behavior of water thus controls the rates of water-coupled protein motions, changing by many orders in magnitude within a narrow range. This is the essence of the dynamical transition observed with hydrated proteins.

In contrast to NMR, neutron scattering yields further information on spatial and temporal behavior of hydration water. Fig. 12 shows the intermediate scattering function $I(q, t)$ of water in the hydration shell of H_2O-hydrated myoglobin at various q-values. The correlation function displays a two-fold decay in time. The amplitude of the fast component at 0.3 ps, increases with q, while the rate is constant. It reflects damped translational oscillations of water molecules. The rate constant of the second process increases with q (spatial resolution).This is a characteristic feature of translational diffusion. For Gaussian displacements, one expects an exponential correlation function with a characteristic rate $1/\tau = q^2 \times D$ with diffusion constant D. Instead, a stretched exponential decay is observed implying the diffusion coefficient to vary with q [54]:

$$I(q,t) = \exp\left[-q^2 \cdot D(q) \cdot t\right]^{\beta} = \exp\left[-q^2 \cdot \langle r^2(q,t)\rangle/6\right] \tag{29}$$

The stretched time-dependence ($\beta < 1$) indicates that the water molecules become attached for some time. When they

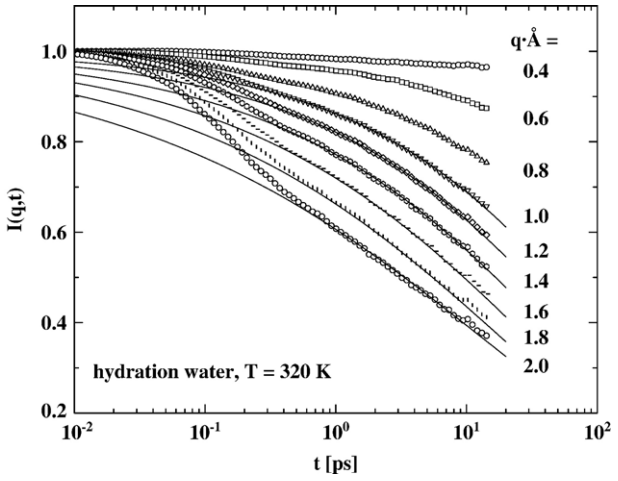

Fig. 12. Density correlation function of myoglobin hydration water at 0.4 g D_2O/g protein and fits to a stretched exponential function, Eq. (28) (Instrument: IN6, ILL) [54].

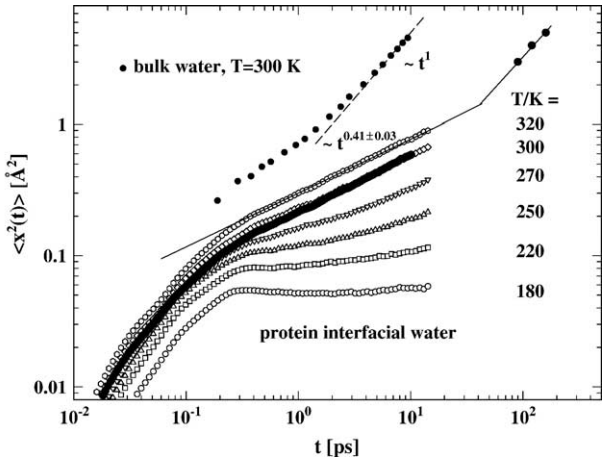

Fig. 13. Time-resolved displacements of bulk water and of myoglobin interfacial water at 0.4 g D_2O/g protein versus temperature (IN6, ILL). Full circles: IN15, ILL.

are released, motional bursts occur. The second equality in Eq. (28) refers to a more general property of $I(q, t)$, which can be expanded in terms of the second and higher moments of the displacement distribution function:

$$I(q,t) = 1 - A_0(t) - \frac{1}{6}q^2\langle \vec{r}^2(t) + \frac{1}{24 \cdot 5} \cdot q^4 \langle \vec{r}^4(t)\rangle - \ldots \tag{30}$$

Adjusting the data to a fourth order polynom yields the second and the fourth moment of the displacement distribution function $G(r, t)$. In practice, one has to account for multiple scattering corrections $A_0(t)$ [54,56].

Fig. 13 shows the resulting mean square displacements of protein interfacial water in comparison with bulk water [54].The data on bulk water by Brockhouse et al. provided the first information on fast motions in a liquid using neutron spectroscopy [57]. After the initial rise due to vibrational dephasing, the displacements of bulk water reach the limiting

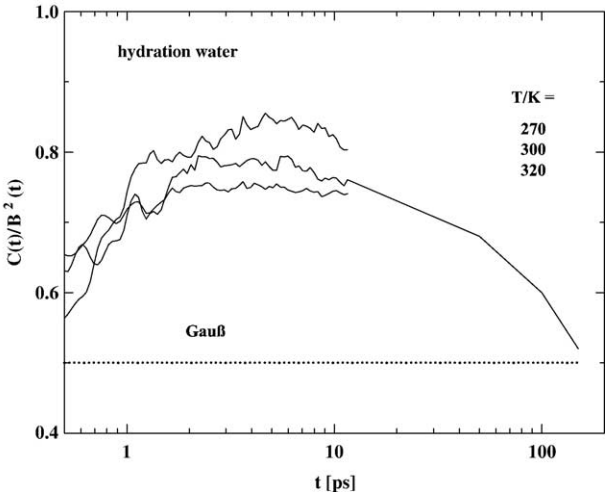

Fig. 14. Gauss deviation $g(t)$ of the hydration water displacement distribution versus time of myoglobin (0.35 g/g) [54].

diffusion region, $\langle x^2\rangle = 2D \times t$, within 10 ps. The slope of the dashed line corresponds to the long time diffusion coefficient of water, $D = 2.45 \times 10^{-5}$ cm^2/s. Note the sublinear regime near 1 ps, reflects the constraints of a water molecule exerted by its nearest neighbors. For interfacial water the sublinear range is drastically extended. Anomalous diffusion is defined by a sublinear power law, $\langle x^2\rangle \propto t^{\alpha}$ with exponent $\alpha < 1$. After about 100 ps, the regime of regular diffusion is reached. The protein thus enhances the cage effect leading to partially localized water states. With decrease in temperature, the cage becomes a trap.

The extended plateau at 180 K is the signature of a solid state. Structural arrest is achieved continuously as the temperature decreases, which excludes discontinuous transitions such as ice formation.

Fig. 14 shows the time dependent fourth moment of the water displacement distribution (Eq. (17)). C/B^2 is Gaussian (0.5) at short times due to vibrational motions. It then increases and goes through a maximum at 8 ps, the local protein–water relaxation time. This indicates (see Fig. 5) that water displacements near the protein surface occur along a preferential direction. However, at times above 100 ps the Gaussian value is re-established, consistent with the observed linear time dependence of the second moment, Fig. 13.

Fig. 15 compares protein and hydration water displacements. The short time level of water was adjusted to the protein displacement at low temperature and the initial rise due to vibrational dephasing is not shown. The data demonstrate that fast protein–water displacements emerge together at the glass transition temperature of hydration water near 180 K [38,39]. But they readily diverge in time with increasing temperature. Above the glass-transition temperature, even short-time protein–water motions are not strictly correlated. Since this effect is not seen with dehydrated samples, we conclude that protein displacements are 'water-assisted' comparable to plasticizers in polymer physics. The figure also shows that the short-time amplitude increases with

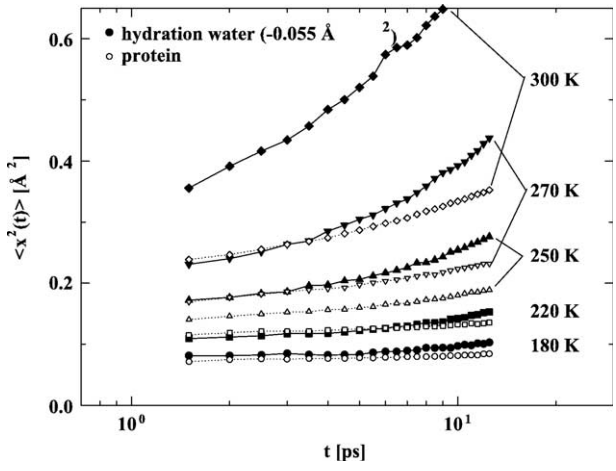

Fig. 15. Comparison of protein-intrinsic and hydration water displacements versus time and temperature. The vibrational plateau of water has been reduced to establish a common level at zero time [42,45].

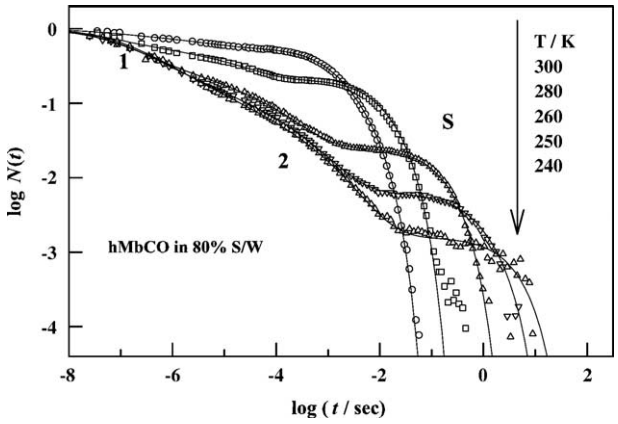

Fig. 16. Kinetics of CO-binding to myoglobin in 80% sucrose–water at different temperatures on a double logarithmic scale [16]. $N(t)$ denotes the fraction of unbound ligand after photolysis. Kinetic components indicated by 1 and 2 are due to internal rebinding, while 'S' reflects overall rebinding of CO molecules from the solvent. The amplitude of process S is equivalent to the CO solvent escape fraction N_S.

the temperature. We assign this process to the fast component in the Figs. 10 and 12. The rate of the β-process is generally weakly temperature-dependent, but its amplitude increases above the glass temperature.

A molecular interpretation refers to open-closed transitions of hydrogen bonds switching allegiances [59]. The α-relaxation process in contrast refers to the elementary translational step [20,21]. The time-scale of this process increases in a super-Arrhenius manner when the glass-temperature is approached. The α-component corresponds to the slow q-dependent process in Fig. 10. The increasing translational constraints at low temperatures lead to an increasing time range of anomalous diffusion, Fig. 13. α and fast β-relaxation are closely related: The rate of the α-process depends on the amplitude of fast hydrogen bond fluctuations. Structural arrest results from increasing the strength of hydrogen bonds, either by lowering the temperature or by adding cosolvents like sucrose: A corresponding discontinuity in the frequency shifts of the O–H stretching vibrations and the amide bands at the glass temperature was observed for myoglobin in various solvents [60].

7. Protein function: heme-ligand displacements

In a biological context, it is of central importance to understand how sidechain and water fluctuations modulate the active site and functional properties such as ligand binding.

Myoglobin is particularly interesting because the kinetics of ligand binding and the dynamics of the heme group were studied in various solvents [16,58]. Fig. 16 shows the kinetics of ligand binding (CO) to myoglobin in a viscous solvent, 80% sucrose–water at various temperatures. Initially, the CO-molecule is bound to the heme iron. A short laser flash brakes the bond. The ligand can either rebind internally or move to the solvent. The fast processes

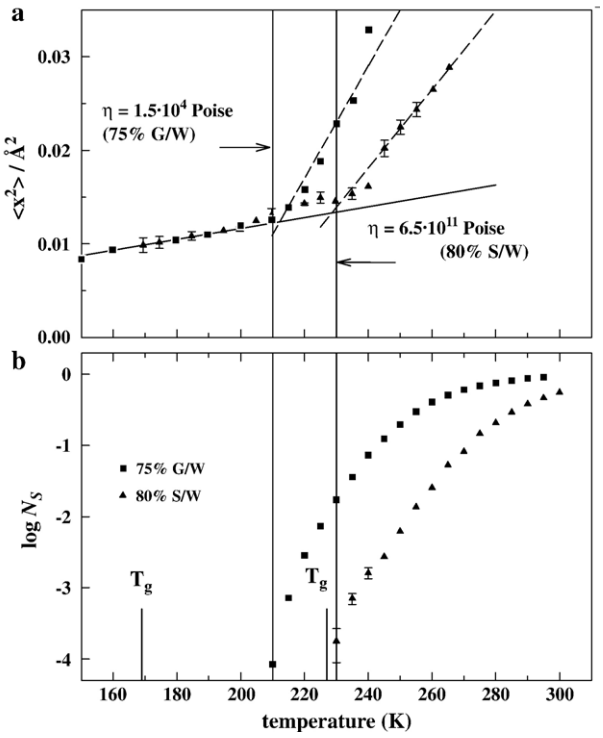

Fig. 17. a) Displacements of the heme iron of ^{57}Fe-substituted myoglobin in either 75% glycerol–water or 80% sucrose–water solution measured with Mössbauer spectroscopy [58] and b) ligand solvent-escape fraction (log N_S) after photolysis, the glass temperatures and the viscosity is indicated.

1 and 2 reflect internal binding, while the component 'S' varies with the CO-concentration in the solvent. The viscosity of the solvent diverges with decreasing temperature, reaching 10^{13} cP at 230 K, the glass temperature of 80% sucrose–water. The viscosity increase causes a drastic reduction in the kinetic amplitude of process S, N_S. Near T_G ligand escape is virtually suppressed. The kinetic fraction of internal rebinding increases in parallel, while the respective rate remains essentially constant. The vitrification of the solvent thus affects ligand transfer rates across the protein–solvent interface, while internal ligand displacements seem to be decoupled from the surface. This result corroborates with the neutron scattering data, where internal motions were rather unaffected by a glassy environment, Fig. 3.

Fig. 17 shows the displacements of the heme iron for two viscous solvents, 75% glycerol-water and 80% sucrose-water versus the temperature derived from Mössbauer resonance absorption spectroscopy [58]. The data refer to a single q-value of 7.2 Å^{-1}. To determine the second moment thus requires a considerable extrapolation to $q = 0$. The resulting apparent displacement, because of the positive curvature of $S_{inc}(q)$, should be interpreted as a minimal value. The observation time, $t_{res} \approx 141$ ns, of the Mössbauer experiment is given by the nuclear life time of the ^{57}Fe nucleus, which is much longer than the 50 ps of the neutron scattering experiment in Fig. 7. The cross-over from harmonic to anharmonic displacements is observed with both methods in the same range of temperatures. Neutron scattering experiments with hydrated and crystalline myoglobin display an onset temperature of 180 K, while deoxymyoglobin crystals observed with Mössbauer spectroscopy show the transition at 205–210 K [18, 58]. The correlation time of hydration water changes in this range by about three orders in magnitude (Fig. 10). The ratio of τ / t_{res} is thus similar for the two methods at the respective onset-temperatures. The data in Fig. 17 demonstrated for first time, that the onset temperature of the dynamical transition increases with the solvent viscosity [58].

At the transition temperature of 220 K, the relaxation time of glycerol water is about 1 μs [16]. Thus, $t_{res}/\tau = 140/1000 = 0.14$, which is compatible with the onset (0.1–0.2) in Fig. 9. This result implies, as with myoglobin crystals [69], that heme displacements and structural fluctuations of the solvent occur on a similar time-scale. However, with sucrose–water as solvent such a correlation could not be established: at the onset temperature of 250 K, one measures a solvent relaxation time of 100 ms, which is orders in magnitude longer than t_{res}. In contrast, the shift in onset temperature correlates quite well with the ligand escape fraction in Fig. 17. N_S reflects the partitioning of internal rebinding and escape to the solvent. The latter depends on the solvent viscosity:

$$N_S = \frac{k_{out}(\eta)}{k_{out}(\eta) + k_{in}} \tag{31}$$

k_{out} and k_{in} are ligand escape rate and internal binding rate. It was shown for a variety of solvents at moderate cosolvent concentrations that $k_{out} \propto \eta^{-1}$ [16]. In contrast with 80% sucrose–water, it was found that $k_{out} \propto \eta^{-\kappa}$ where $\kappa < 1$, a partial decoupling from the bulk viscosity. Taken together these results indicate that the effective surface viscosity is likely to be lower than in the bulk. If the standard chemical potential of the co-solvent near protein surface is larger than in the bulk, a compensation occurs by decreasing the respective concentration. Thermodynamic analysis of various co-solvents has shown that carbohydrates like sucrose are

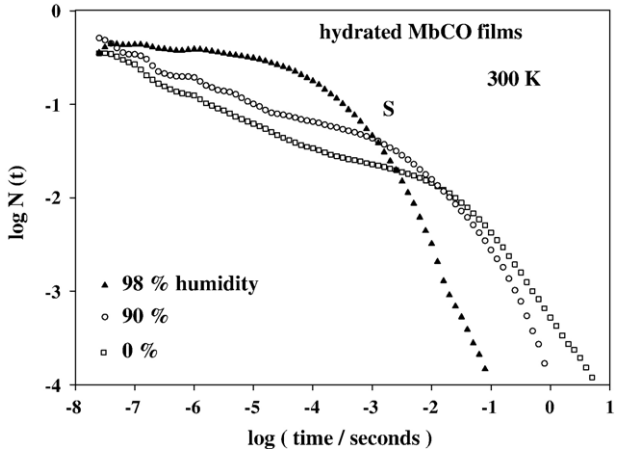

Fig. 18. Kinetics of CO-binding to spin-coated hydrated myoglobin films, S denotes rebinding from the hydration shell [26,65].

preferentially excluded from the protein-domain [61]. Preferential hydration is the most likely explanation of the reduced surface viscosity. The geminate binding rates are viscosity independent, which indicates that heme displacements are not directly involved in the formation of the covalent bond. It has been proposed, however, that the dynamic disorder of the heme position contributes to the observed spread in the binding rates [58].

Finally, we come back to the dehydrated glassy state of proteins: The neutron-scattering spectra of myoglobin in different environments (Fig. 3) demonstrate that embedding a protein in a rigid solvent or removing the solvent entirely reduces small-scale liquid-like motions. The two environments correspond however to opposing limits in viscosity. In particular, the solvent friction should diminish with decreasing hydration. The relaxation rate of a damped harmonic oscillator initially increases with friction at low damping, while it decreases at high damping. The lubricating action of water, the rate enhancement, is thus a likely result of an increasing solvent friction in the low damping regime. Fig. 18 shows the kinetics of CO-binding to myoglobin in spin-coated films at various degrees of hydration [26,65]. The kinetics observed at 98% humidity closely resemble CO-recombination in solution. A decrease in humidity lowers the escape fraction and enhances internal rebinding. Internal ligand displacements are thus not suppressed by dehydration. The neutron-scattering data suggest that ligand migration couples to side-chain torsional motions, which occur in the dry state. Moreover, even after dehydration of several weeks in a P_2O_5 atmosphere, escape to a long-lived solvent-like state is possible. This result points to a finite effective viscosity, which is lower than in the glass as suggested above.

8. Conclusions

Dynamic neutron scattering experiments probe the statistical properties of fast motions in biomolecules. To understand the effect of water on structure and stability of proteins requires to study the interactions on a picosecond time-scale where hydrogen bonds are broken and formed. With neutron scattering, one essentially records the average trajectories of protein–water hydrogens. The method thus complements more local probes like NMR and fluorescence emission. The momentum exchange in the scattering process provides additional spatial information. Based on a general moment analysis, one can derive time-dependent displacement distribution functions. Two types of protein displacements could be discriminated: torsional transitions and continuous, water-assisted motions. The latter are composed of fast H-bond fluctuations and slower small scale displacements. The former are not seen with D_2O-hydrated protein samples, because H-bond motions involve mainly the exchangeable hydrogens. Experiments with hydrogenated samples suggest that the rapid increase in amplitude of H-bond fluctuations with temperature correlates with the anharmonic enhancement of protein displacements [10,17,38,60]. The transition is a genuine property of the tight protein–water coupling, which modifies both protein and water. There is neither a master nor a slave. The transition temperature thus varies with H-bond strength and viscosity [58,60]: the temperature shift of vibrational frequencies of amide I and the O–H stretching vibration of hydration water display a discontinuity near the glass temperature of the solvent [17,60]. This shows that the average strength of protein hydrogen bonds decreases above T_G due to anharmonic fluctuations. The fraction of ‘open’ hydrogen bonds, which is an equilibrium property, becomes noticeable above this temperature. In other words the amplitude of fast hydrogen bond fluctuations (β-processes) have reached a critical value. This softening effect drastically lowers the characteristic time of long range translational diffusion [17,20]. Probing the glass transition with increasing instrumental time resolution will thus lower the apparent transition temperature not indefinitely. The lower limit is given by the temperature, where the β-processes have reached a critical amplitude. The respective critical temperature, which is independent of t_{res} plays a central role in mode coupling theory of glass-forming liquids [20,64]. Note the pretransition in the displacements of the heme iron in sucrose/water at 200 K (Fig. 17), which may reflect a separation of fast β-processes and the time-scale sensitive structural α-relaxation. A true glass transition always involves the arrest of long-range translational diffusion. In the native state, protein-residues can only perform localized motions, which is the characteristic feature of a molecular glass. Thus, compact proteins will not undergo a glass-transition. By using the term ‘protein-dynamical transition’, we imply that a particular fraction of local motions freezes due to viscous coupling to structural coordinates of the glass-forming solvent [37,38]. The term transition is justified by the fact that a dynamical quantity, the relaxation time of water, changes by many orders in magnitude within a small range of temperatures.

To classify protein motions as α- or β-processes is misleading [15,37,66]. Rather, one should argue that particular protein-displacements are coupled to fast β-processes (H-bond fluctuations) or to the slow structural α-relaxation (translation) of water. Close to the glass transition, solvent and protein motions freeze in parallel on the same time scale. However, at higher temperatures, the role of the solvent reduces to a frictional force, which fluctuates on a much faster time scale than protein-collective motions. This type of coupling can be treated using a generalized Langevin-equation, where the friction is frequency dependent due to colored noise of random solvent forces [67,68]. The generalized Langevin equation serves as the basis of a microscopic theory of the liquid to

glass transition [20]. The term 'slaving' implies that a fast coordinate adjusts adiabatically to a slow coordinate: electrons follow the nuclear adjustments on the same time scale. The opposite is true for protein–water interactions: water reorientational dynamics occur on a much faster time scale than protein collective displacements, which implies 'viscous' coupling and not 'slaving' [3]. Moreover, we have seen that the hydration shell and not the bulk phase couples to protein motions in contrast to what is suggested in ref. [66]. The protein energy landscape is not self-trapping, as proclaimed to the contrary for a long time, but needs a solvent to freeze. Protein dynamics is thus not derivable from an intrinsic-free energy surface. Instead, one should discuss the protein–solvent seascape. Structural rearrangements correlated with motions of water molecules occur on a time scale of picoseconds. In what sense is then the fast motion of water molecules relevant to the observed slow substrate conversion in enzymes? For myoglobin, it could be shown that the solvent modulates the barrier controlling ligand entry and escape according to Kramers law of activated escape [16,58]. The solvent generates the seascape of fluctuating barriers.The transfer rates vanish in a super-Arrhenius manner with decreasing temperature. Thus given enough time, ligand escape across the protein–solvent interface will occur even below T_G, however, with orders in magnitude lower probability than above the glass transition. Moreover, intramolecular ligand displacements and binding proceed at high rate far below the glass transition of the solvent. It is thus not surprising that Daniel et al. [51,52] observe enzymatic activity below the dynamical transition of the protein. While protein fluctuations are measured with picosecond time resolution, enzyme turn-over times in the range of seconds are recorded. Moreover, the most relevant parameter, the viscosity of their methanol–water solvent, did not increase drastically between room temperature and 200 K. The plasticizing action of water to protein structural displacements seems to be rather similar to the self-plasticization of water as a liquid: changing allegiances of hydrogen bonds between donors and acceptors [59]. Structural plasticity is thus dominated by polar interactions.

The displacements of molecules on a microscopic scale including water molecules in the active site are discontinuous and always fast. The millisecond time scales come about by high energetic or entropic barriers which prevent particular rearrangements for long-time intervals. Enzymes are thus devices, which select by construction a small fraction of events out of a large number of fast structural fluctuations.

Acknowledgements

The authors are grateful for technical support by the instrument responsibles of the Institut Laue Langevin (Grenoble), the Hahn Meitner Institut (Berlin) and the collaboration with many colleagues. Financial support by the Bundesministerium für Bildung und Forschung (grant 03DOE2M) and the Deutsche Forschungsgemeinschaft (SFB 533) are gratefully acknowledged.

References

[1] K.A. Dill, Dominant forces in protein folding, Biochemistry 29 (1990) 7132–7155.
[2] I. Iben, D. Braunstein, W. Doster, H. Frauenfelder, M. Hong, J. Johnson, S. Luck, P. Ormos, A. Schulte, P. Steinbach, A. Xie, R. Hong, Glassy behaviour of a protein, Phys. Rev. Lett. 62 (1989) 1916–1919.
[3] P.W. Fenimore, H. Frauenfelder, B.H. McMahon, F.G. Parak, Slaving, solvent fluctuations dominate protein dynamics and functions, Proc. Natl. Acad. Sci. U. S. A. 99 (2002) 16047–16051.
[4] G. Zaccai, How soft is a protein, Science 288 (2000) 1604.
[5] W. Doster, M. Diehl, W. Petry, M. Ferrand, Elastic resolution spectroscopy: a method to study molecular motions in small biological samples, Physica, B 301 (2001) 65–68.
[6] W. Doster, M. Diehl, R. Gebhardt, R.E. Lechner, J. Pieper, Time-of-Flight elastic resolution spectroscopy, time domain analysis of weakly scattering samples, Chem. Phys. 292 (2003) 487–494.
[7] J.C. Smith, Protein dynamics, comparison of simulations with inelastic neutron scattering experiments, Q. Rev. Biophys. 24 (1991) 227–291.
[8] J.A. Hayward, J. Smith, Temperature dependence of protein dynamics, Biophys. J. 82 (2002) 1216.
[9] M. Tarek, T. Tobias, Single particle and collective dynamics of protein hydration water, Phys. Rev. Lett. 89 (2002) 13801.
[10] M. Tarek, T. Tobias, The role of protein–water hydrogen bonds in the dynamical transition of proteins, Phys. Rev. Lett. 88 (2002) 381011–381013.
[11] M. Tarek, G.J. Martyna, T. Tobias, J. Am. Soc. 122 (2000) 10450.
[12] M. Tarek, D. Tobias, The dynamics of protein hydration water, a quantitative comparison of molecular dynamics simulations and incoherent neutron scattering experiments, Biophys. J. 79 (2000) 3244–3257.
[13] H. Frauenfelder, G.A. Petsko, D. Tsernoglou, Temperature-dependent x-ray diffraction as a probe of protein structural dynamics, Nature 280 (1979) 558–563.
[14] H. Hartmann, F. Parak, W. Steigemann, G.A. Petsko, D. Ringe-Ponzi, H. Frauenfelder, Conformational substates in a proteins, structure and dynamics of met-myoglobin at 80 K, Proc. Natl. Acad. Sci. U. S. A. 79 (1982) 4967–4971.
[15] J.L. Green, J. Fan, A. Angell, The protein glass analogy, J. Phys. Chem. 98 (1994) 13780–13790.
[16] Th. Kleinert, W. Doster, H. Leyser, W. Petry, V. Schwarz, M. Settles, Solvent composition and viscosity effects on the kinetics of ligand binding to horse myoglobin, Biochemistry 37 (1998) 717–733.
[17] W. Doster, M. Settles, Protein dynamics, the role of hydrogen bonds, Hydration Processes in Biology, (Nato Science Series A Life Science, Vol 305, IOS Press, Ed. MC Bellisent-Funel, 1998) pp. 177–194 and 375 (http://www.e13.physik.tu-muenchen.de/Doster).
[18] F. Parak, E.W. Knapp, D. Kucheida, Protein dynamics: Mossbauer spectroscopy on deoxy myoglobin crystals, J. Mol. Biol. 161 (1982) 177–194.
[19] F. Gabel, D. Bicout, U. Lehnert, M. Tehei, M. Weik, G. Zaccai, Protein dynamics studied by neutron scattering, Qu. Rev. Biophys. 35 (2002) 1.
[20] W. Götze: Aspects of structural glass transition in Liquids, Freezing and Glass Transition, Les Hounches: Part II, in: J.P. hansen, North Holland, 1989, p. 287.

[21] W. Götze, L. Sjögren, Mode-coupling theory for supercoolded liquids, Rep. Prog. Phys. 55 (1992) 241–376.
[22] H. Wang, A. Ben-Naim, Solvation and solubility of globular proteins J, Phys. Chem., B 101 (1997) 1077–1086.
[23] L. Slade, H. Levine, J.W. Finley, in: R.D. Phillips, J.W. Finley (Eds.), Protein Quality and the Effects of Processing, Marcel Dekker, New York, 1989, pp. 9–121.
[24] R.B. Gregory, Protein hydration and glass transition behaviour, in: R.B. Gregory (Ed.), Protein-Solvent Interactions, Marcel Dekker, New York, 1995, p. 191.
[25] R. Pethig, Dielectric studies of protein hydration, in: R.B. Gregory (Ed.), Protein-Solvent Interactions, Marcel Dekker, New York, 1995, p. 265.
[26] W. Doster, Th. Kleinert, F. Post, M. Settles, Effect of Solvent on proteininternal dynamics, The kinetics of ligand binding to myoglobin, in: R.B. Gregory (Ed.), Protein-Solvent Interactions, Marcel Dekker, New York, 1995, p. 375.
[27] H. Batzer, U.T. Kreibich, Polym. Bull. 5 (1981) 585.
[28] J. Wong, C.A. Angell, Glass Structure by Spectroscopy, Marcel Dekker, New York, 1976, p. 743.
[29] A. Paciaroni, S. Cinelli, G. Onori, Effect of the environment on the protein dynamical transition, Biophys. J. 83 (2002) 1157–1164.
[30] W. Doster, M. Diehl, H. Leyser, W. Petry, H. Schober, Terahertz spectroscopy of proteins, in: J. Greve, G.J. Puppels, C. Otto (Eds.), Spectroscopy of Biological Molecules, Kluwer Acad. Pub, 1999, pp. 655–659.
[31] J. Fitter, R. Lechner, G. Büldt, N.A. Dencher, Internal motions of proteins by incoherent neutron scattering using oriented purple membranes, Proc. Natl. Acad. Sci. U. S. A. 93 (1996) 7600–7605.
[32] J. Fitter, R. Lechner, N.A. Dencher, Pico-second motions of bacteriorhodopsin investigated by neutron scattering, Biophys. J. 93 (1997) 2126–2137.
[33] J.M Zanotti, M.C. Bellissent-Funel, J. Parello, Hydration-coupled dynamics in proteins studied by neutron scattering and NMR, Biophys. J. 76 (1999) 2390.
[34] M. Ferrand, A. Dianoux, W. Petry, G. Zaccai, Thermal motions and function of bacteriorhodopsin in purple membranes, Proc. Natl. Acad. Sci. U. S. A. 90 (1993) 9668.
[35] U. Lehnert, V. Reat, M. Weik, G. Zaccai, C. Pfister, Hydration level and protein dynamics, Biophys. J. 75 (1998) 1945–1952.
[36] M.C. Bellissent-Funel, J.M. Zanotti, S.H. Chen, Slow dynamics of water molecules on the surface of a protein, Faraday Discuss. 103 (1996) 281–294.
[37] W. Doster, S. Cusack, W. Petry, Dynamic transition of myoglobin revealed by inelastic neutron scattering, Nature (London) 337 (1989) 754.
[38] W. Doster, T. Bachleitner, M. Hiebl, E. Lüscher, A. Dunau, Thermal properties of water in myoglobin crystals and solutions, Biophys. J. 50 (1986) 213–219.
[39] W. Doster, Glass transition of hydration water and structural flexibility of myoglobin, in: A. Ehrenberg, R. Rigler, A. Gräslund, L. Nilsson (Eds.), Structure, Dynamics and Function of Biomolecules, Springer Series in Biophysics, vol. 1, 1986, p. 34.
[40] M. Bee, Quasielastic Neutron Scattering, Adam Hilger, Bristol, PA, 1988, p. 16.
[41] W. Marshall, S.W. Lovesey, Theory of Thermal Neutron Scattering, Clarendon Press, Oxford, 1971.
[42] M. Settles, Time dependence and geometry of intramolecular dynamics of globular proteins up to 100 ps from neutron scattering experiments, Thesis, Technical University Munich, Munich, 1997.
[43] J.L. Barrat, J.N. Roux, J.P. Hansen, Mode coupling theory for the glass transition, Chem. Phys. 149 (1990) 197–208.
[44] P. Gallo, F. Sciortino, P. Tartaglia, S.H. Chen, Slow dynamics of water in supercooled states, Phys. Rev. Lett. 76 (1996) 2730–2745.
[45] W. Doster, Analysis of Molecular Motions in Biomolecules, in: Th. Gutberlet, J. Fitter (Eds.), Neutrons in Biology, Methods, and Application, Springer Verlag, 2005, (in press).
[46] H. Nakagawa, H. Kamikubo, I. Tsukushi, T. Kanaya, M. Kataoka, J. Phys. Soc. Jpn. 73 (2004) 491–495.
[47] L. Cordone, M. Ferrand, E. Vitrano, G. Zaccai, Harmonic behaviour of trehalose-coated carboxy-myoglobin at high temperature, Biophys. J. 76 (1999) 1043–1047.
[48] G. Kneller, W. Doster, M. Settles, S. Cusack, J. Smith, Methyl group dynamics in the crystalline alanine dipaptide, J. Chem. Phys. 97 (1992) 8864–8879.
[49] A. Lee, J. Wand, Microscopic origins of entropy, heat capacity and the glass transition in proteins, Nature 411 (2001) 501.
[50] D.J. Bicout, G. Zaccai, Protein flexibility from the dynamical transition, Biophys. J. 80 (2001) 1115–1123.
[51] R.M. Daniel, J.L. Finney, V. Rat, R. Dunn, M. Ferrand, J. Smith, Enzyme activity below the dynamical transition, Biophys. J. 77 (1999) 2184–2190.
[52] R.M. Daniel, J.L. Finney, V. Rat, R. Dunn, M. Ferrand, J. Smith, Enzyme dynamics and activity, the time scale dependence, Biophys. J. 75 (1999) 2504–2507.
[53] D. Di Cola, A. Deriu, M. Sampoli, A. Torcini, Dynamical properties of liquid water, J. Chem. Phys. 104 (1996) 4223–4232.
[54] M. Settles, W. Doster, Anomalous diffusion of adsorbed water, a neutron scattering study of hydrated myoglobin, Faraday Discuss. 103 (1996) 269–279.
[55] M. Settles, W. Doster, F. Kremer, F. Post, W. Schirmacher, Proton conductivity and bound water reorientation in hydrated myoglobin, Phila. Mag. B65 (1992) 861–866.
[56] M. Settles, W. Doster, Iterative calculation of the vibrational density of states from incoherent neutron scattering data, in: H. Büttner (Ed.), Biological Macromolecular Dynamics, Adenine Press, 1996, pp. 3–8.
[57] M. Sakamoto, B.N. Brockhouse, R.G. Johnson, N.K. Pope, Neutron inelastic scattering study of water, J. Phys. Soc. Jpn. 17 (1962) 370–376.
[58] H. Lichtenegger, W. Doster, T. Kleinert, B. Sepiol, G. Vogl, Heme-solvent coupling, a Mossbauer study of myoglobin in sucrose, Biophys. J. 76 (1999) 414–422.
[59] A. Luzar, Water–hydrogen bond dynamics close to hydrophobic and hydrophilic groups, Faraday Discuss. 103 (1996) 29–40.
[60] F. Demmel, W. Doster, W. Petry, A. Schulte, Vibrational frequency shifts as aprobe of hydrogen bonds. Europ. Biophys. J. 26 327–335. (1999) 375.
[61] G. Xie, S.N. Timasheff, The thermodynamic mechanism of protein stabilization by trehalose, Biophys. Chem. 64 (1997) 25–43.
[62] R.J. Loncarich, B. Brooks, J. Mol. Biol. 215 (1990) 439–455.
[63] W. Doster, S. Cusack, W. Petry, Dynamic instability of liquid-like motions in a globular protein, Phys. Rev. Lett. 65 (1990) 1080.
[64] W. Doster, The glass transition anomalies of myoglobin in the light of mode coupling theory, Mod. Phys. Lett. B 5 (1991) 1407.
[65] Th. Kleinert, W. Doster, F. Post, M. Settles, Hydration effects on protein function, the kinetics of ligand binding to myoglobin, in: M.U. Palma, M.B. Palma-Vitorelli, F. Parak (Eds.), Water–Biomolecule Interactions, Societa Italiana di Fisica, 1992, p. 127.
[66] P.W. Fenimore, H. Frauenfelder, B.H. McMahon, R.D. Young, Bulk solvent and hydration shell fluctuations, similar to α-an d β-fluctuations in glasses, control protein motions and functions, Proc. Natl. Acad. Sci. U. S. A. 101 (2004) 14408–14413.
[67] H. Leyser, W. Doster, M. Diehl, Far infrared emission by boson peak oscillations in globular protein, Phys. Rev. Lett. 82 (14) (1999) 2897.
[68] W. Doster, Viscoelastic structural relaxation in proteins, in Hydration Processes in Biology, NATO Science Series 305 1999.
[69] G.P. Singh, F. Parak, S. Hunklinger, K. Dransfeld, Role of absorbed water in the dynamics of metmyoglobin, Phys. Rev. Lett. 48 (1981) 685–688.